Journal of Medicinal Chemistry



Article

# Toward Selective Histone Deacetylase Inhibitor Design: Homology Modeling, Docking Studies, and Molecular Dynamics Simulations of Human Class I Histone Deacetylases

Di-Fei Wang, Paul Helquist, Norbert L. Wiech, and Olaf Wiest

*J. Med. Chem.*, **2005**, 48 (22), 6936-6947• DOI: 10.1021/jm0505011 • Publication Date (Web): 12 October 2005



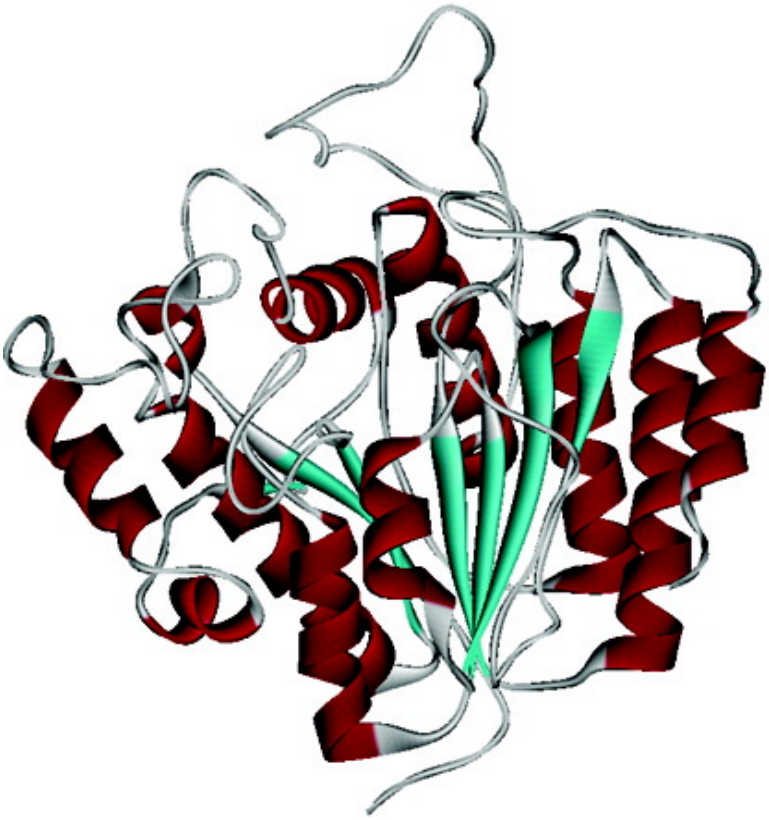

## More About This Article

Additional resources and features associated with this article are available within the HTML version:

- Supporting Information
- Links to the 12 articles that cite this article, as of the time of this article download



Journal of Medicinal Chemistry is published by the American Chemical Society. 1155 Sixteenth Street N.W., Washington, DC 20036

# Toward Selective Histone Deacetylase Inhibitor Design: Homology Modeling, Docking Studies, and Molecular Dynamics Simulations of Human Class I Histone Deacetylases

Di-Fei Wang,[†] Paul Helquist,[†] Norbert L. Wiech,[‡] and Olaf Wiest[†,*]

*Walther Cancer Research Center and Department of Chemistry and Biochemistry, University of Notre Dame, Notre Dame, Indiana 46556-5670, and Errant Gene Therapeutics, 200 West Jackson Boulevard, Suite 2400, Chicago, Illinois 60606*

*Received May 27, 2005*

Histone deacetylases (HDACs) play an important role in gene transcription. Inhibitors of HDACs induce cell differentiation and suppress cell proliferation in tumor cells. Although many HDAC inhibitors have been designed and synthesized, selective inhibition for class I HDAC isoforms is a goal that has yet to be achieved. To understand the difference between class I HDAC isoforms that could be exploited for the design of isoform-specific HDAC inhibitors, we have built three-dimensional models of four class I histone deacetylases, HDAC1, HDAC2, HDAC3, and HDAC8. Comparison of the homology model of HDAC8 with the recently published X-ray structure shows excellent agreement and validates the approach. A series of HDAC inhibitors were docked to the homology models to understand the similarities and differences between the binding modes. Molecular dynamic simulations of these HDAC−inhibitor complexes indicate that the interaction between the protein surface and inhibitor is playing an important role; also some active site residues show some flexibility, which is usually not included in routine docking protocols. The implications of these results for the design of isoform-selective HDAC inhibitors are discussed.

## Introduction

Modification of the $\epsilon$-amino group of specific lysines within histones by acetylation and deacetylation plays a crucial role in the transcriptional process.[1] Two families of enzymes, acetyl transferases and deacetylases, are involved in controlling the acetylation state of histones. Many recent studies show that inhibition of histone deacetylases (HDACs) elicits anticancer effects in several tumor cells by inhibition of cell growth and inducing cell differentiation. As a result of these findings, several programs for the development of HDAC inhibitors as anticancer drug have been initiated. Natural products such as the hydroxamic acid trichostatin A (TSA)[2] and the cyclic tetrapeptides apicidin[3] and trapoxin[4] as well as synthetic inhibitors,[5] such as suberanilo hydroxamic acid (SAHA)[6] or the simplified TSA analogue CG-1521 (Chart 1),[7] have been studied in cancer cell lines and in tumor animal models[8] in order to develop new approaches to cancer chemotherapy.[9]

Detailed biochemical studies show that there are four classes of histone deacetylases. Class I and II HDACs are zinc-containing hydrolases. Eleven mammalian HDAC genes have been found so far.[10,11] HDAC1, HDAC2, HDAC3, and HDAC8 are the members of class I and are related to the yeast RPD3 gene product. Traditionally, HDAC 11 was also counted as a member of this class. However, a recent phylogenetic analysis revealed it to be in the separate class IV, which diverged very early in prokaryotic evolution.[12] Class II contains HDAC4, HDAC5, HDAC6, HDAC7, HDAC9, and HDAC10, homologues of the yeast HDAC1 protein. Class III is a series of the NAD-dependent Sir2 family of enzymes.[13] They are structurally and evolutionarily unrelated to the other HDAC classes. Accumulating biological data suggest that each member of the HDAC family is a component of a physical complex playing a distinct role in gene expression. For instance, retinoblastoma tumor suppressor protein is associated with a large protein complex containing HDAC1 and E2F transcription factor[14] while HDAC4 and HDAC5 are associated specifically with myocyte enhancer factor MEF2A and repress MEF2A-dependent transcription.[15] Recent data also indicate that a variety of other cancer-

**Chart 1.** Some Known HDAC1 Inhibitors

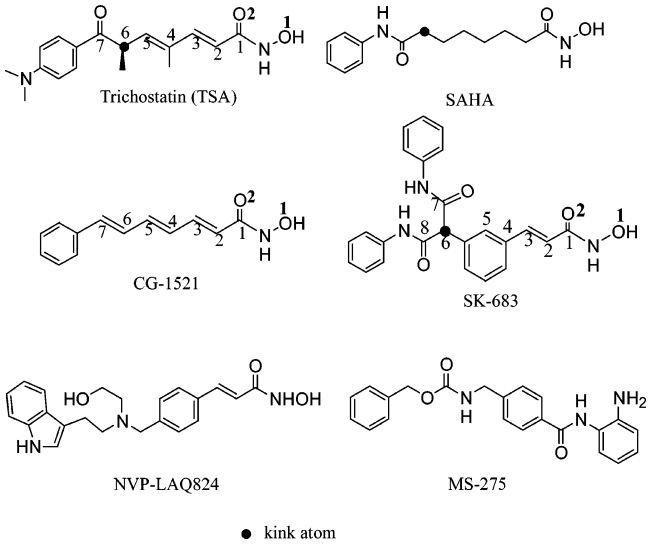


* To whom correspondence should be sent. Phone: (574) 631 5876, Fax: (574) 631 6652, e-mail: owiest@nd.edu.
† University of Notre Dame.
‡ Errant Gene Therapeutics.

10.1021/jm0505011 CCC: $30.25 
Published on Web 10/12/2005

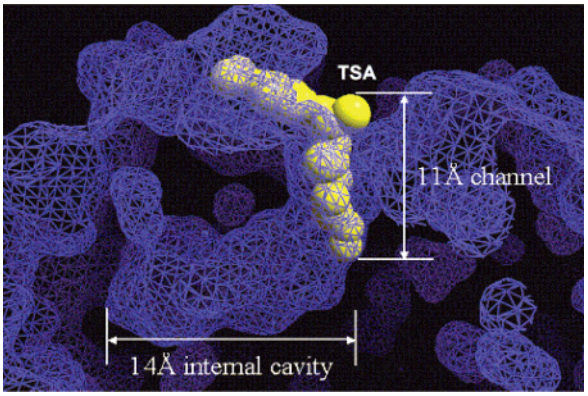


**Figure 1.** Surface representation of the 11 Å channel and the 14 Å internal cavity of the HDLP−TSA complex. TSA is displayed as yellow CPK model.[8]

related proteins, including p53, are also substrates of HDACs.[7d,16]

The X-ray crystal structures of an HDAC homologue, histone deacetylase-like protein, HDLP, from *A. aeolicus* and its TSA and SAHA complexes were first elucidated with 2.0 Å resolution.[17] It revealed that HDLP has a tube-like, 11 Å deep channel (called the channel afterward) which leads to the active site and which accommodates the lysine side chain in the natural substrate and TSA or SAHA in the protein−inhibitor complexes (Figure 1). A catalytic zinc ion is at the bottom of this channel. The aliphatic chain of TSA or SAHA has multiple favorable contacts with hydrophobic residues in the channel. Interestingly, there is a 14 Å long side pocket (called the internal cavity afterward) adjacent to the $Zn^{2+}$ binding site. The role of this internal cavity, which is conserved across a range of class I HDACs was not elucidated in the original publication. Subsequent docking calculations from our group[7a] suggested that it accommodates the acetate after hydrolysis and can potentially act as a second binding site. A sequence alignment shows a 35.2% sequence identity of HDLP and human HDAC1 (Figure 2), with similarly high homologies to other members of HDAC class I. The residues around the HDLP $Zn^{2+}$ binding site are completely conserved in all human class I HDACs. All of the hydrophobic residues that make up the 11 Å channel in HDLP are also identical in the four class I HDACs shown in Figure 2. With one exception, the residues making up the 14 Å internal cavity are either identical or conservatively substituted across the different class I HDACs. As can be expected from the high degree of sequence similarity shown in Figure 2, class I HDACs have the same structural features as HDLP described above. As will be discussed later, this relationship is confirmed by the excellent agreement between the homology models derived from sequence alignment and the recently published X-ray structures of HDAC8. [18]

Although the exact mechanism by which HDACs selectively regulate specific genes is poorly understood, it is obvious that the selective inhibition of specific HDACs over others is highly desirable and more likely to yield specific and nontoxic drugs. This goal has been frequently stated,[9b] but the high similarity of the residues in the channel, active site, and internal cavity of all class I HDACs means that other parts of the proteins will also have to be considered for the design of isoform-specific inhibitors. In particular, it is not clear whether currently investigated HDAC inhibitors such as the ones shown in Chart 1 have the potential of being isoform-specific, whether inhibitors with larger surface contact areas such as apicidin have more potential, or more subtle differences between isoforms can be exploited. The results so far indicate that this is a very challenging task. For example, the most extensively studied inhibitor, TSA, unselectively inhibits all Class I and II HDACs.[19] One of the most severe obstacles for the design of rational design of selective HDAC inhibitors is the lack of three-dimensional structures of human HDACs. In recent years, homology modeling techniques have been proven to predict three-dimensional protein structures with a considerable accuracy if the template structure and the target structure have above 30% residue identity, and their sequences have been well-aligned.[20] The generation and refinement of homology models for different HDACs could therefore provide a starting point for the design of specific inhibitors.

In this paper, we present homology models of four Class I human HDACs (HDAC1, HDAC2, HDAC3, and HDAC8) that are validated by comparison with the X-ray structure of HDAC8 which became available during the course of our study. The similarities and differences between the isoforms were then probed by docking three known HDAC inhibitors (TSA, SK-683, and CG-1521) into each of the homology models. In addition, three HDAC inhibitors that are currently in clinical trials are docked to the three most diverse homology models. Finally, the dynamic behaviors of these HDAC−ligand complexes have been studied through a series of molecular dynamics simulations. These results provide new information for designing isoform-selective HDAC inhibitors.

## Computational Methodology

**Sequence Alignment and Homology Modeling.** Sequences of Human HDAC1 (Genbank Accession Number Q13547,482aa), HDAC2 (Genbank Accession Number AAH-31055,488aa), HDAC3 (Genbank Accession Number AAH-00614,428aa), HDAC8(Genbank Accession Number AAH-50433,377aa), and histone deacetylase-like protein (HDLP, Genbank Accession Number 1C3P_A,375aa) were extracted from the NCBI protein sequence database. All sequences were imported into the ClustalW program[21] and the sequence alignment editor, BioEdit,[22] for multiple pairwise alignments. The resulting alignments were examined manually. The three-dimensional structure of HDLP (PDB code: 13CR) was used as a template for human HDACs homology modeling in the Modeler7 program.[23a] Electrostatic Surfaces were generated using the Delphi module of InsightII with the Charmm27 force field, a grid spacing of 0.5 Å, and dielectric constants of 2 and 80 for the solute and the solvent, respectively.

**Molecular Docking.** AutoDock 3.0[24] was used for all docking calculations. The AutoDockTools[25] package was employed to generate the docking input files and to analyze the docking results. A grid box size of $90 \times 90 \times 90$ points with a spacing of 0.375 Å between the grid points was implemented and covered almost the entire HDAC protein surface. For TSA and other inhibitors, the single bonds except the amide bond were treated as active torsional bonds (see all structures in Chart 1). One hundred docked structures, i.e. 100 runs, were generated by using genetic algorithm searches. A default protocol was applied, with an initial population of 50 randomly placed individuals, a maximum number of $2.5 \times 10^5$ energy evaluations, and a maximum number of $2.7 \times 10^4$ generations.

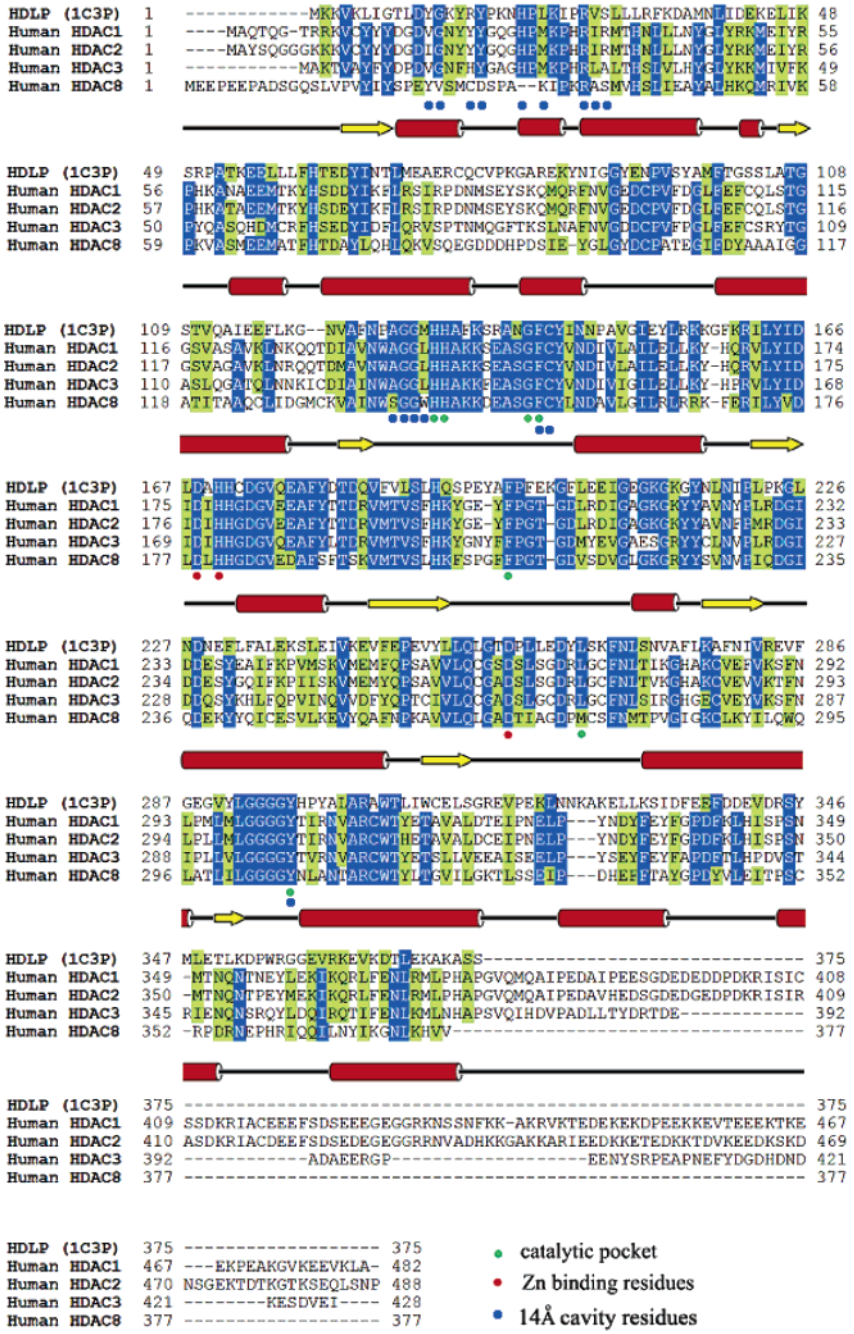


**Figure 2.** Sequence alignment of *A. aeolicus* HDLP (histone deacetylase-like protein) and class I human HDACs (HDAC1, HDAC2, HDAC3, and HDAC8). The secondary structure assignment was derived from the HDLP structure. Catalytic residues, $Zn^{2+}$-binding residues, and residues forming the 14 Å internal cavity are marked as green, red, and blue dots, respectively.

A mutation rate of 0.02 and a crossover rate of 0.8 were used. Results differing by less than 0.5 Å in positional root-mean-square deviation (RMSD) were clustered together and represented by the result with the most favorable free energy of binding. The RMSD value reported in this work is an all heavy atom comparison between the docked structure and the initial structure.

The xleap module in Amber8 package[26] was used to generate the missing hydrogens for HDACs models. The united partial charges for protein atoms were taken from the standard Amber force field. The partial charges for all docked ligands were derived from two-step electrostatic potential (ESP) calculations in the Amber8 package using HF/6-31G* wave functions obtained by single point calculations in G98.[27] These ligand partial charges were further modified by using the AutoDockTools package so that the charges of the nonpolar hydrogen atoms were assigned to the atom to which the hydrogen is attached.

The choice of the scoring function is a crucial decision in any docking study, and a large number of comparative studies have appeared in the literature. On the basis of the many successful examples of structures of protein−ligand,[28] protein−protein,[29] and protein−oligosugar[30] systems and the limited inclusion of ligand flexibility, which is important for adequate docking to the constrained active site of HDACs, we chose the AutoDock docking protocol and scoring function. There are only a few examples of docking studies of metalloprotein−ligand systems in the literature.[31] This paucity is due to the difficulty in finding the proper force field parameters for metal centers in metalloproteins. Since for the purpose of flexible docking calculations a nonbonded model for a metal center is more realistic than a bonded one, we used the nonbonded $Zn^{2+}$ parameters of Stote et al.[32] which were used successfully in several molecular dynamics studies.[33] This approach has been validated in our previous work[7a] that showed excellent agreement between calculated and experimental binding constants

($R^2$ = 0.91) for seven inhibitors ranging over 5 orders of magnitude in activity.

**Molecular Dynamics Simulations.** The Sander module of Amber8[26] was used for molecular dynamics (MD) simulations. Starting from the initial structures obtained by the docking studies, standard Amber02 force field parameters were assigned to the HDAC protein structures using xleap. General Amber Force Field (GAFF) parameters were assigned to ligands. The partial charges for all ligands were derived from restrained electrostatic potential[34] (RESP) calculations as described above. All ligands were given a total formal charge of 0. Equivalent atoms were assigned to equal partial charges. The nonbonded model for a $Zn^{2+}$ was chosen to allow the change of coordination number during the simulation.[32]

Protein−ligand systems were solvated by a cubic box of TIP3P waters,[35] which extended at least 15 Å away from any given protein atoms. Systems were setup for simulations with the Particle Mesh Ewald (PME) method for treating long-range electrostatic interactions, a 10 Å cutoff for nobonded van der Waals interactions, and periodic boundary conditions. All bonds involving hydrogen atoms were constrained using the SHAKE algorithm. The time step of 2 fs was used to integrate the equations of motion. Systems were minimized by holding protein structure with a force of 50 kcal·m$^{-1}$ with the combination of 2500 steps of steepest descent and 2500 steps of conjugated gradients. Systems were gradually heated to 300K in 15000 steps by imposing a force of 5 kcal m$^{-1}$. Then, the systems were equilibrated at 300K for 30ps and followed by another 30 ps with PME treatment. Finally, the systems were run for 1 ns of production simulation at constant temperature (300 K) and pressure (1 atm) with the Berendsen coupling algorithm with a time constant for heat bath coupling of 0.2 ps. The ptraj module in Amber8 and the WebLab4.0 program were used to analyze and visualize the structures and MD trajectories.

## Results and Discussion

**Sequence Alignment and Homology Models Validation.** The final result of multiple sequence alignment of the HDACs is shown in Figure 2. HDAC1, HDAC2, HDAC3, and HDAC8 share the same active site and zinc binding residues with HDLP. The differences between HDAC1 and HDAC2 are very small with a 85% sequence identity and 93% sequence similarity (using the similarity matrix PAM250[36]) while HDAC1 and HDAC3 are slightly more distinct with a 52% sequence identity and 73% sequence similarity. The percentages of identity and similarity drop to 53% and 31% when HDAC1 and HDAC8 are compared. The ability to distinguish between the isoforms is expected to correlate with these differences, i.e., HDAC1 and HDAC2 will be hard to distinguish whereas sequence differences between HDAC1 and HDAC8 could be exploited by suitable inhibitors.

In addition to the highly homologous regions, HDAC1, HDAC2, and HDAC3 have additional segments in their C-terminal domains that are about 50−110 amino acids long. When these portions of the sequences were subjected to a BLAST search at the NCBI website, no alignment was possible, and no similar sequences (other than themselves) were found. The function of these residues was proposed to recruit other enzymes to large protein complexes that may regulate their activities.[37] Therefore, they may have less influence on the substrate/inhibitor binding. Due to the lack of structural information on these portions, they were omitted in the further study.

After sequence alignment of the HDACs, 10 models for each of the four HDACs were generated through the Modeler7 program.[21a] The resulting models were further optimized with the MD function implemented in Modeler. The quality of the models thus obtained was then evaluated with respect to the conformation of the peptide backbone and the packing environment. Generation of the Ramachandran plots using Procheck[21b,c] (for plots, see Supporting Information) gave no residues having Phi/Psi angles in the disallowed ranges, and the percentage of residues having Phi/Psi angles in the most favorable ranges is around 90%, similar to the template structures used. The quality of Ramachandran plots was satisfactory for all of the models. In the second test, the packing environments for residues of the same type in high quality experimental structures (<2 Å resolution) deposited in the Protein Data Bank were compared with our HDAC models using WHAT IF.[38] A score of −5.0 or worse usually indicate poor packing. In general, our HDAC models have similar packing scores compared to the template X-ray structure. A few residues (see plots in the Supporting Information) are poorly packed in these models based upon scores less than −5.0. However, these values were again similar to the ones in the template structure. In summary, the quality of our HDACs models has been checked by two different criteria. The results showed that our models are reliable for performing further docking and MD studies.

**Comparison of the Homology Model and X-ray Structure of HDAC8.** During our homology modeling studies of HDACs, the X-ray structures of human HDAC8 cocrystallized with several inhibitors were reported at 1.9 and 2.5 Å resolution.[18] Comparison of the X-ray structures to our homology model of HDAC8 offers another, independent way of validating our results and provides a "worst case" scenario for the other homology models because HDAC8 has the largest sequence difference compared to the HDLP template. The overlay of the two structures, together with the analysis of the secondary structure for each of the residues as generated by Stride[39] is shown in Figure 3.

With a backbone RMSD of 2.07 Å for residues 14−324, the HDAC8 homology model is very similar to the X-ray structure 1T69. The overall secondary and tertiary structures are very similar for the model and the X-ray structure. This also includes the loops adjacent to the active site (located at the center in Figure 3). The only major differences between the two 3D structures as identified by Stride are located in the region from Asp333 to Leu346 because of the sequence diversity between HDLP and HDAC8 in this region. In particular, the homology model displays a series of continuous turns while the X-ray structure displayed only coils.

Our earlier docking study of HDLP[7a] proposed that the internal cavity accepts the hydrolyzed acetate, which would then depart upon opening of flexible residues at the end of the cavity. It was thus gratifying to note that the internal cavity is exposed to the outside environment in one of the X-ray structures of HDAC8 but it is closed in the other structures. This indicates that there is some flexibility of this side of the cavity. It could be either opened or closed depending on the structural difference of inhibitors. Our molecular dynamics simulation study of the X-ray structure of HDAC8[40] shows that this region is quite flexible and the cavity could be opening and closing during the time scale of our MD simulation. In the HDAC8 model shown, this cavity is

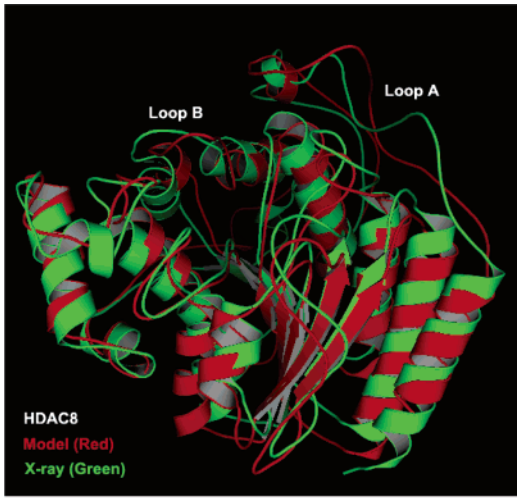


```
1    LVPVYIYSPEYVSMCDSLAKIPKRASMVHSLIEAYALHKQMRIVKPKVAS   50
       EEE  HHHHHHHH TTTTTTHHHHHHHHHHHH GGGG EEE
      EEEE  GGGGG   TTTTT   HHHHHHHHHHH    GGGEE
51   MEEMATFHTDAYLQHLQKVSQEGDDDHPDSIEYGLGYDCPATEGIFDYAA  100
     HHHHHTTT HHHHHHHHHHHHHTTTTTTTTGGG  BTTBT TTTHHHHHH
     HHHHHHH  HHHHHHHHHHHHH   TTTTTTTTTTTTTTT TTTTTHHHH
101  AIGGATITAAQCLIDGMCKVAINWSGGWHHAKKDEASGFCYLNDAVLGIL  150
     HHHHHHHHHHHHHHHTTTTEEEETTT TTTTBTTB BTTBTTTHHHHHHH
     HHHHHHHHHHHHHHHHTTTTEEEETTT TTTTTTTT BTTBTTTHHHHHHH
151  RLRRKFERILYVDLDLHHGDGVEDAFSFTSKVMTVSLHKFSPGFFPGTGD  200
     HHHH TTTEEEEE    TTHHHHHHHTTTTTEEEEEEE TTTTTTT  T
     HHHHH   EEEEE      HHHHHHHH TTTEEEEEEEETTTTTTTTTT
201  VSDVGLGKGRYYSVNVPIQDGIQDEKYYQICESVLKEVYQAFNPKAVVLQ  250
     TTT   GGGTTTEEEEEETTTT HHHHHHHHHHHHHHHHHH TTEEEEE
     TTT  TTTTTTTEEEEEETTTT HHHHHHHHHHHHHHHHHH  TTEEEEE
251  LGADTIAGDPMCSFNMTPVGIGKCLKYILQWQLATLILGGGGYNLANTAR  300
       TTTBTTTTTT   B HHHHHHHHHHHHHH   EEEE   TTTHHHHHH
       TTTBTTTTTT   B HHHHHHHHHHHHHHH   EEE      HHHHHH
301  CWTYLTGVILGKTLSSEIPDHEFFTAYGPDYVLEITPSCRPDRNEPHRIQ  350
     HHHHHHHHH      B   TTTGGGGTTTTB             HHHHH
     HHHHHHHHH      B   HHHHH    TTTTTT   TTTBTTT
351  QILNYIKGNLKHVV                                    364
     HHHHHHHHHH
        HHHHHHHHH
```

**Figure 3.** Secondary structures and fold comparison between the homology model and the X-ray structure of HDAC8 (first line: sequence, starting at Leu14; second line: fold in x-ray 1T64; third line: fold in homology model). E: $\beta$-strand; H: $\alpha$-helix; T: turn; G: $3_{10}$-helix; B: breaker.

not directly exposed to the exterior. The detailed study of this region demonstrates that a two-residue deletion subtly changed the loop B structure by rotating one lysine residue, which covers the cavity in the homology model, out of its normal position. Another large conformational difference between our model and the X-ray structure of HDAC8 was found in loop A, about 20−30 residues long, residing between the last helix and the second to last one. In our model, multiple turns exist in this loop while it is largely a random coil in the X-ray structure as shown in Figure 3. We are currently investigating the flexible opening of the internal cavity as a potential second binding site for HDAC inhibitors. Such inhibitors should then display significant selectivity for HDAC8 because of a much lower flexibility of this loop in the other isoforms.

**Discussion of the Homology Models.** Ramachandran plots, packing analysis, and comparison of one of the homology models to the X-ray structure suggests that the homology models will be good predictors of the actual structures. The overall folds of the HDACs models are quite similar. In all four models studied, a single $\alpha/\beta$ domain that includes an eight-stranded parallel $\beta$ sheet sandwiched between 13 and 17 helices is displayed. Almost half of the residues are involved in these secondary structures, while the other half exists in the loops and turns which link these secondary structures together. The residues that are critical for catalysis appear in several loops adjacent to the active site and are highly conserved, leading to essentially identical active sites in the different class I HDACs. It is therefore unlikely that the binding pocket itself can be exploited to achieve isoform selectivity. Instead, an analysis of the interactions on the surface could identify motifs that could be used to understand selective binding. Figure 4 shows the Delphi-generated electrostatic surfaces of the two available X-ray structures as well as the four HDAC homology models.

The environment in the direct vicinity of the channel exit shows some small differences that might be used to differentiate among isoforms. In particular, the surface of HDAC8 in this area is less polar than that of HDAC1, while that of the remaining two class I HDACs are of intermediate polarity. It is also noteworthy that the surface charges agree fairly well between our model and the experimental structure of HDAC8. The largest differences in surface potentials among the class I HDACs occur in areas far away from the active site. For example, it can be seen in Figure 4 that HDAC1 and HDAC2 display considerably more positive charge on the face containing the active site entry point than HDAC3 or HDAC8. These differences could be responsible for the selective recruitment of other proteins that allow the HDACs to target specific genes or specific lysines on other proteins such as p53.[7d]

**Docking of Inhibitors to HDACs Models.** The findings presented above suggest that the structural basis for class I isoform selectivity can be elucidated by docking of different HDAC inhibitors to the isoforms. It is known in the literature that the majority of HDAC inhibitors do not differentiate between class I HDACs. They should therefore have very similar binding modes for the different HDACs discussed here. Conversely, HDAC inhibitors that show isoform selectivity should have different binding modes. To investigate this hypothesis, we docked several different hydroxamic acid-based HDAC inhibitors to the four homology models. TSA is thought to be a strong inhibitor of all class I HDACs, as indicated by $IC_{50}$ values of $\sim$0.2 $\mu$M for HDAC1, HDAC3, and HDAC8.[41] SK-683 was selected as a potent inhibitor that makes surface contacts using symmetric groups. Finally, we chose our lead compound, CG-1521, which does not make surface contacts due to the rigid backbone.

The results for TSA, SK-683, and CG-1521 are shown in Figure 5 while the calculated binding energies are summarized in Table 1. As expected, TSA binds in the active site of HDAC1, HDAC2 and HDAC3 with a similar pattern. All docked TSA structures have the same orientation as in the X-ray structure of the HDLP−TSA cocrystal. The hydroxamic acid group, attached with its long aliphatic chain lying in the 11 Å channel, binds to the zinc atom at the bottom of this channel. The aromatic ring is close to either a Glu or an Asp residue. For SK-683 in HDAC1, the two identical

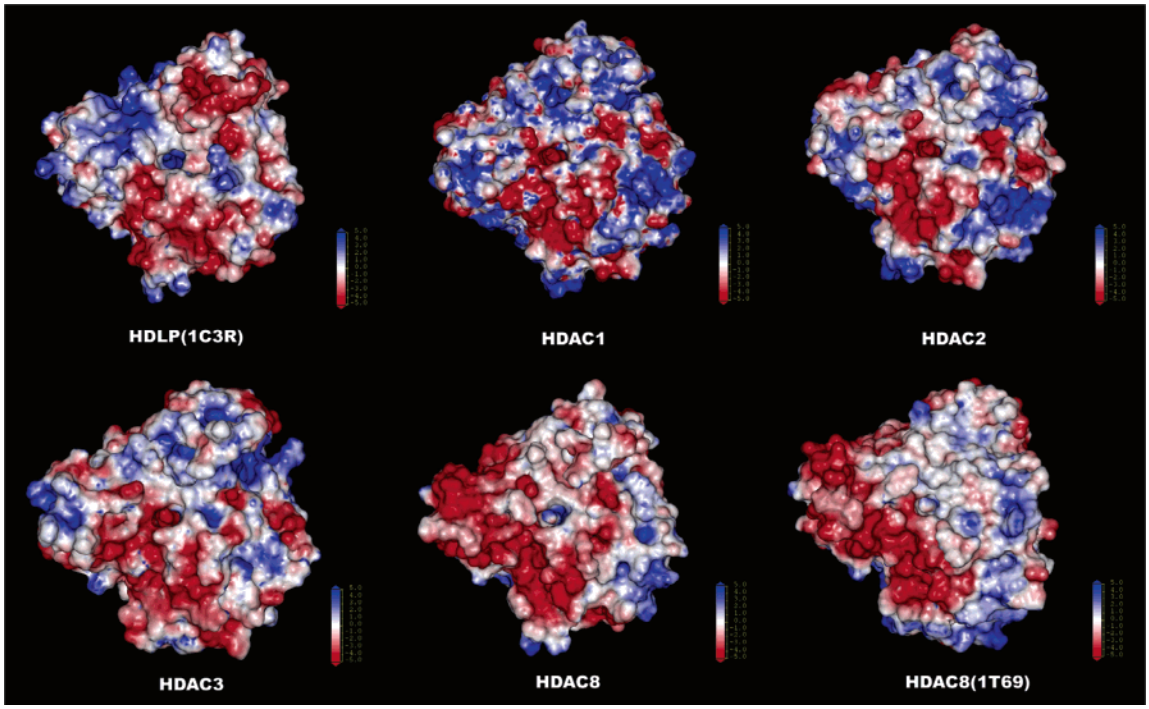


**Figure 4.** Electrostatic surfaces on a scale of +5 to −5 for homology models and X-ray structures of HDLP and HDACs 1, 2, 3, and 8.

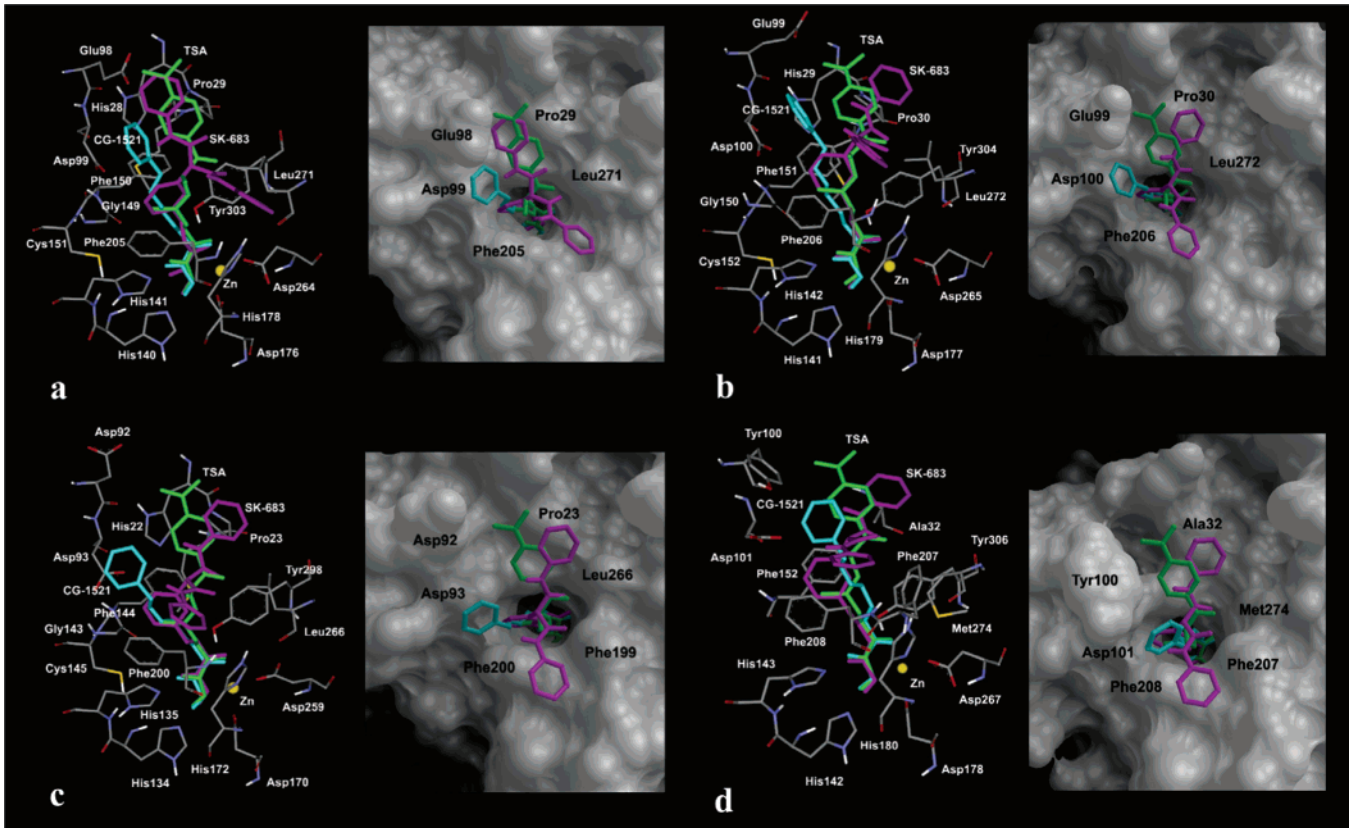


**Figure 5.** Structures of docked TSA (green), SK-683 (purple) and CG-1521 (cyan) in the active sites of HDAC1 (a), HDAC2 (b), HDAC3 (c), and HDAC8 (d) (left) and their top views in these proteins with surface representations (right).

aromatic groups are in contact with regions A and C described in our previous work,[7a] while these groups are shifted slightly to regions B and C in HDAC2 and HDAC3. CG-1521 binds straight into the 11 Å channel, and its aromatic tail points directly out in all four HDAC proteins.

The estimated free energy of binding of TSA in the docked structure is about −10.1 kcal/mol for HDAC1. For SK-683, it is about −11.5 kcal/mol. This result agrees with the experimental observation of stronger binding of SK-683 compared to TSA and CG-1521 to HDAC1. Therefore, the estimated free energies of bind-

**Table 1.** Calculated and Experimental $\Delta G_{binding}$ (in kcal/mol)

| | | $\Delta G_{binding(calcd)}$ | $\Delta G_{binding(exp)}$ | $N^a$ |
|---|---|---|---|---|
| HDAC1 | TSA | −10.1 | −10.3 | 29 |
| | | | −9.0[d] | |
| | SK-683 | −11.5 | −12.3 | 11 |
| | CG-1521 | −8.7 | −7.8 | 3 |
| | SAHA | −8.3 | −8.6 | 1 |
| | MS-275 | −11.5 | −8.9[d] | 1 |
| | NVP-LAQ824 | −8.8 | NA[b] | 1 |
| HDAC2 | TSA | −10.1 | NA[b] | 29 |
| | SK-683 | −10.0 | NA[b] | 8 |
| | CG-1521 | −8.6 | NA[b] | 3 |
| HDAC3 | TSA | −10.4 | −9.0[d] | 27 |
| | SK-683 | −10.5 | NA[b] | 1 |
| | CG-1521 | −8.3 | NA[b] | 1 |
| | SAHA | −9.2 | NA[b] | 1 |
| | MS-275 | −12.2 | −7.0[d] | 1 |
| | NVP-LAQ824 | −11.0 | −10.2[c] | 1 |
| HDAC8 | TSA | −9.9 | −9.0[d] | 43 |
| | SK-683 | −10.7 | NA[b] | 4 |
| | CG-1521 | −8.1 | NA[b] | 11 |
| | SAHA | −8.2 | NA[b] | 1 |
| | MS-275 | −11.2[e] | no activity[d] | 6 |
| | NVP-LAQ824 | −9.4 | NA[b] | 1 |

[a] *N* is the number of structures in the first cluster except CG-1521. For CG-1521, *N* is the number of structures in the clusters. [b] Not available. [c] Reference 42, HDAC only partially purified. [d] Reference 41. [e] $\Delta G_{binding(calcd)}$ for second binding pocket, value for active site binding is −8.9 kcal/mol

ing of TSA to HDAC2 and HDAC3 agree with such observations. All three inhibitors have shown small differences in binding energies for HDAC1, HDAC2, and HDAC3, but such difference are in the range of error of the scoring function used, as shown in our previous work.[7a] From the results presented there, it is clear that the scoring function is sufficiently accurate to distinguish between nanomolar and micromolar inhibitors.

Next, we applied the method to three HDAC inhibitors that are in clinical trials: SAHA is one of the best-studied simple hydroxamic acids and has progressed to phase II clinical development against cutaneous T cell lymphoma. The structure of the complex between SAHA and HDAC8 was solved at 2.9 Å resolution.[18a] MS-275 is in phase I trials and was chosen for our present study as one of the very few known class I isoform specific HDAC inhibitors.[18b,41] Finally, NVP-LAQ824[42] is in phase I trials against solid tumors and has been identified in our screening procedure as a potential isoform specific inhibitor. These three inhibitors were docked to the homology models of HDAC1 and HDAC3. For the case of HDAC8, the high-resolution X-ray structure by Somoza et al. was used in the docking.[18a] The calculated binding energies are shown in Table 1, and the docked structures are shown in Figure 6.

In analogy to the findings for TSA, SK-683, and CG-1521, the position and computed binding energies of SAHA is very similar in the three homology models and is very close to the experimental and computed structures of the complex between HDLP and SAHA.[7a] However, a direct comparison between the computed HDAC8−SAHA complex with the experimental structure is difficult because of the poor resolution of the X-ray structure, which leads to several undefined residues in the active site region, as well as well as the fact that in the X-ray structure, the protein adopts a different conformation that closes the second binding site. In agreement with the available experimental data, SAHA binds to the active site and is found to be a weaker inhibitor of HDACs than TSA. The differences in binding energies between the isoforms are again smaller than the expected error of the method. SAHA is therefore not expected to exhibit significant isoform selectivity. In contrast, MS-275 is described as a strong inhibitor of HDAC1 ($IC_{50} \sim 0.3\ \mu M$) and a good inhibitor of HDAC3 ($IC_{50} \sim 8.3\ \mu M$) in one study,[41] while another finds essentially equal inhibition of HDAC1 and HDAC3 by MS-275.[18b] Both studies agree that it is not an inhibitor of HDAC8. Although the calculated binding energies of this benzamide-type inhibitor are not as well validated as the binding energies of the hydroxamate inhibitors and are therefore considered to be quantitatively less reliable, the calculated binding energies are in better agreement with an equal inhibition of HDAC1 and HDAC3.[18b] More importantly, the bonding mode shown in Figure 6c reveals the structural origin of the absence of activity of MS-275 in HDAC8. MS-275 does not bind to the active site, but rather to the cavity adjacent to the active site. This is in analogy to the results of Somoza,[18a] which also indicate that this cavity can act as a second binding site. However, in the case of MS-275, binding to the secondary site is approximately 2 orders of magnitude stronger than binding to the active site. Encouraged by these results, we investigated other known HDAC inhibitors to find class I

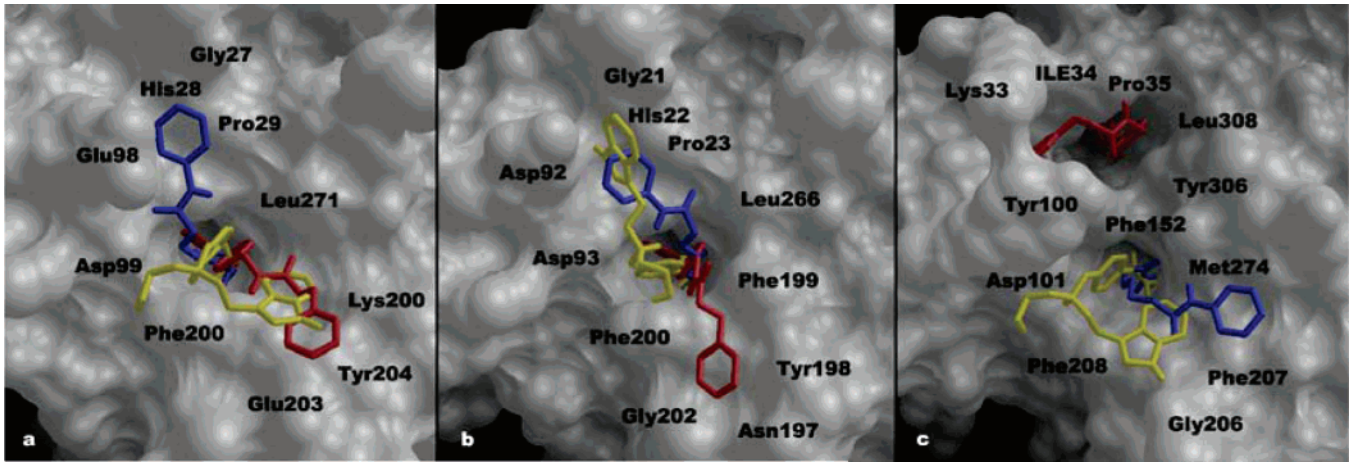


**Figure 6.** Structures of docked SAHA (blue), MS-275 (red), and NVP-LAQ824 (yellow) in the active sites of HDAC1 (a), HDAC3 (b), and HDAC8 (c).

isoform-selective inhibitors. Hydroxamic acid NVP-LAQ824 was calculated to bind stronger to HDAC3 than to HDAC1. Analysis of the different binding modes shown in Figure 6 suggests the origin of the difference in binding constants. Small changes in the binding pocket at the exit of the active site caused by the change of Glu98 in HDAC1 to Asp92 in HDAC3 result in a change in orientation of the indolyl side chain of NVP-LAQ824 and a stronger binding to HDAC3. Although these initial results will have to be verified experimentally and analyzed in more detail by molecular dynamics simulations, they provide insights into the types of studies that can be used for the identification of isoform specific class I HDAC inhibitors and make NVP-LAQ824 a potential lead compound for the selective inhibition of HDAC3. Comparison of the computed results with the $IC_{50}$ of 32 nM[42] reported for a partially purified, unidentified HDAC from H1299 lung carcinoma cells also suggest that the isoform studied there might be HDAC3. In combination with the results for MS-275, these results demonstrate that virtual screening of a large structure database holds promise to find novel, selective class I HDAC inhibitors.

**Molecular Dynamics Simulations of Models of HDAC−Inhibitor Complexes.** While the docking methodology used to study the binding of the HDAC inhibitors allows for flexibility of the ligands, it does not include protein mobility. In a very constrained active site such as that of HDACs, this could lead to very strong repulsive interactions. In addition, the docking calculations do not properly sample the conformational space that could lead to a variety of different binding modes of the ligands.[43] We have therefore performed 1 ns molecular dynamics simulations of HDACs, and their inhibitors were found to be stable under NPT conditions using AMBER8. After equilibration, all complexes converged and were stable in this time frame as indicated by monitoring temperature, density, pressure, and total energy over the course of the simulation (see Supporting Information). RMSD fluctuations of backbone atoms during MD simulations are also often used as an indication of stability of inter- and intradomain movements in protein systems and were found to be small in the systems studied. For the inhibitor complexes of TSA, SK-683, and CG-1521 with HDAC1, HDAC2, and HDAC3, RMSDs were calculated for protein backbone heavy atoms (CA, N, C). For example, in the complex of HDAC1−TSA, the backbone RMSD varies by 2.5 Å during the complete 1 ns simulation, with the majority of the movement occurring in the first 100 ps (see Supporting Information). It can thus be stated that the MD simulations of the different complexes are reasonable representations of the system.

As discussed earlier, the use of a nonbonded model allows the geometry and coordination number around metal ions to change during the course of the simulation. To check whether the zinc coordination and number are reasonable, they were monitored during the course of the MD simulations. Analysis of the simulation trajectory shows that the zinc coordination number and geometry could therefore probe for whether the hydroxamic acids act exclusively as bidentate ligands or if other modes of binding might be possible as suggested by the asymmetric bond lengths observed in the highest resolution X-ray structure of a HDAC−inhibitor complex, 1T69 (2.00 Å and 2.22 Å).[18a] A monodentate coordination would suggest that a number of nonchelating functional groups could also serve as zinc binding moieties.

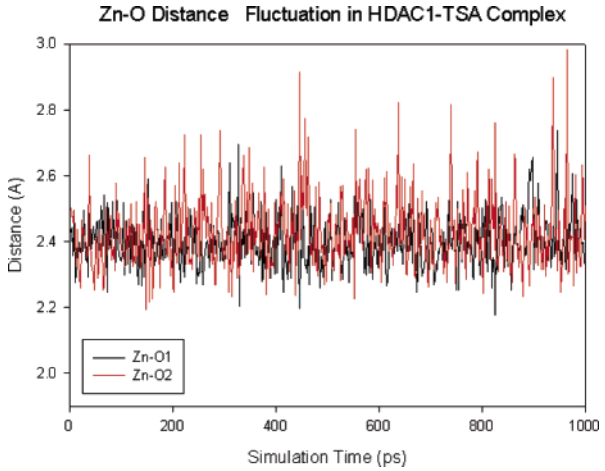


**Figure 7.** $Zn^{2+}$−oxygen distances in HDAC1−TSA complex.

The results for the TSA−HDAC1 complex shown in Figure 7 are typical for all of the HDAC-inhibitor complexes. The $Zn^{2+}$−O1 and $Zn^{2+}$−O2 distances oscillate around 2.4 and 2.5 Å during the 1 ns simulation time. These values match the X-ray results (2.25 and 2.45 Å in Chain A of HDLP−TSA complex 1C3R) quite well. The coordination number of $Zn^{2+}$ is 5 including one His and two Asp residues, as found in the X-ray structures. Interestingly, the more rigid inhibitor CG-1521 showed different behavior in two of the cases. As shown in Figure 8, the coordination number changed for HDAC1−CG-1521 and HDAC3−CG-1521 during the simulation time frame. The $Zn^{2+}$−O1 distance remains at 2.5 Å in the first 600 ps and changed to 4.7 Å in the last 400 ps in the HDAC1−CG-1521 complex. In the HDAC3−CG-1521 complex, the average $Zn^{2+}$−O1 distance is 2.5 Å in the first 728 ps and is elongated to 4.2 Å in the remaining 272 ps, leading to a tetracoordinated zinc ion. This change in the coordination number allows for a better fit of the triene system of CG-1521 in the 11 Å channel. It also suggests that possibility of replacing the bidentate hydroxamic acid residue by other metal binding groups.

The sequence alignment of the four class I HDACs showed that all residues forming the active sites are located in loops, suggesting that the entry channel is fairly flexible. This flexibility is not considered by the docking calculations, but it can be studied in the MD simulations. Figure 9 shows a picture of 21 snapshots of the active site of the HDAC1−TSA complex in the time frame of 400−600 ps. TSA forms close contacts with Phe142, Tyr295, His132, and His133. In agreement with the small changes in the $Zn^{2+}$−oxygen bonds shown in Figure 7, the movement of the zinc-binding residues His170, Asp168, and Asp256 is also relatively minor. In contrast, significant movements are observed for Phe197. In the X-ray structure of the HDLP−TSA complex, the 4-methyl group on TSA is sandwiched between Phe197 and Phe142. Our simulations show that Phe197 is quite flexible and can easily move to accommodate larger groups such as the *N*-methylpyrole moiety in APHA-8 or the phenyl ring in SK683 while maintaining the stacking with Phe142. This high flex-

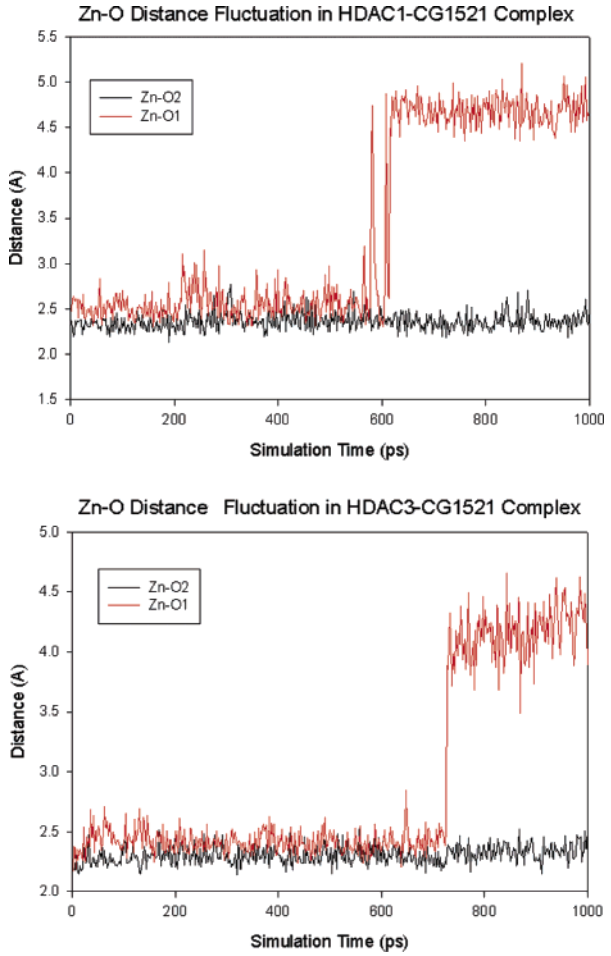


**Figure 8.** $Zn^{2+}$−oxygen distances in HDAC−CG-1521 complex.

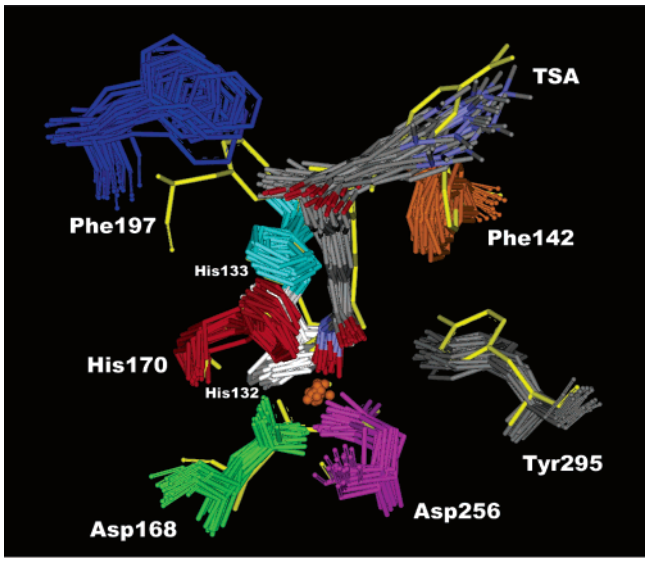


**Figure 9.** Twenty-one active site snapshots selected from 400 to 600 ps for the HDAC1−TSA complex. The orange ball represents the $Zn^{2+}$ ion. Residues shown in yellow correspond to the starting positions in the 1 ns simulation.

ibility was also observed in other simulations of HDAC−TSA complexes, indicating that this interaction is common and could be used to improve binding constants[43].

As shown in Figure 5, HDACs have several pockets available for interactions at the surface of the protein. The MD simulations allow the exploration of the conformational space of the aromatic moieties of the inhibitors. For this purpose, Figure 10 shows a radial plot of the appropriate dihedral angles in the HDAC1−TSA, HDAC1−SK-683, and HDAC1−CG-1521 complexes as a function of the simulation time. Similar plots for HDAC2 and HDAC3 systems are included in the Supporting Information.

In the HDAC1−TSA complex, the dihedral angle prefers to lie in the range of 90° to 120°. This allows the electron-rich *N*,*N*-dimethylaminobenzyl group to interact with a single pocket on the HDAC1 surface. Interestingly, only binding to one of the pockets is observed during the simulation time or in the docking, indicating that the positioning of the *N*,*N*-dimethylaminobenzyl between Pro29 and Glu98 is more favorable than the alternative sites. In contrast, HDAC1−SK-683 is more flexible. While one of the aromatic rings (denoted with dihedral angle 1 in Figure 10) maintains surface contact at all times, the second aryl group has little surface interactions and a wide angle distribution. This suggests that there is little binding interaction of this group with the surface, and that the binding constant could be further improved by addition of a more flexible linker. The increased binding constant of SK683 compared to TSA is most likely due to the binding interaction with Phe197 discussed earlier. For the HDAC2 and HDAC3 systems, a similar pattern was observed but the actual values differ. In agreement with the qualitative considerations from Figure 4, this suggests that the surface of HDAC3 is more different from that of HDAC1 than that of HDAC2. Hence, this result would be helpful for further rational design of selective inhibitors for different HDAC isoforms.

It is clear from Figure 10 that CG-1521 shows a very different conformational behavior. All dihedrals have a very narrow angle distribution, resulting from the conjugation of the side chain and the fact that the triene portion is inserted straight into the 11 Å channel with no contacts between the HDAC1 surface and the aromatic group. This may also partially explain the relative inhibition activity of SK-683 > TSA > CG-1521. Introduction of more aromatic groups around the kink atom would enhance the binding activity.[40] This conclusion agrees with our previous docking study.[7a]

## Summary

The three-dimensional models for four class I histone deacetylases (HDAC1, HDAC2, HDAC3, and HDAC8), which were built using homology modeling and validated by bioinformatics techniques and by comparison to an X-ray structure not used in the generation of the models, were docked to three widely studied HDAC inhibitors (TSA, CG-1521, and SK683). Three more HDAC inhibitors that are in clinical trials (SAHA, MS-275, and NVP-LAQ824) were docked to HDAC1, HDAC3, and HDAC8. The high homology of the class I HDACs in the active site region and the 11 Å channel make it unlikely that the small differences in these parts of the enzyme can be exploited to achieve isoform selectivity. However, small differences in the shape and charge distribution around the opening of the active site hold

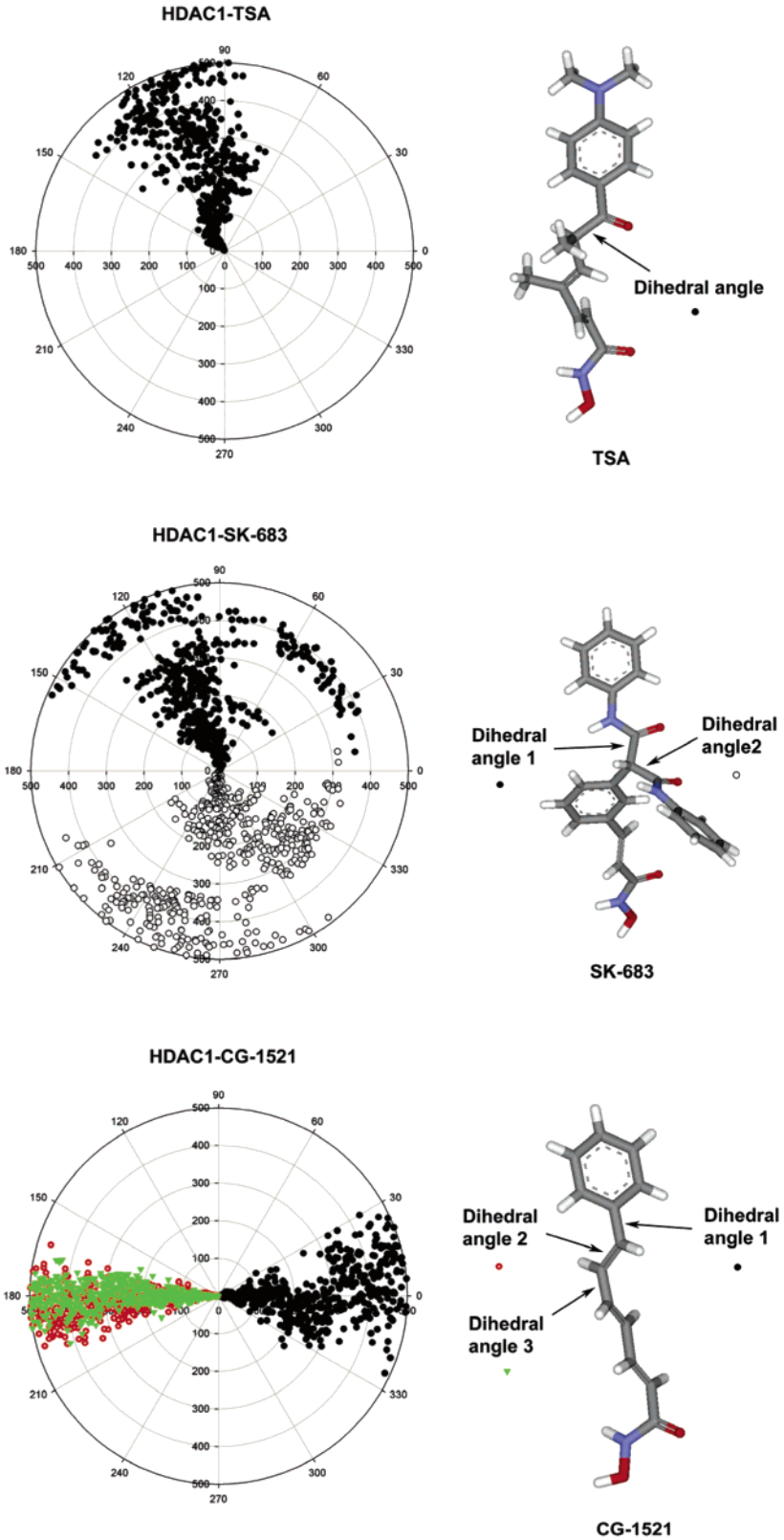


**Figure 10.** Selected dihedral angles of inhibitors describing the conformational changes of the cap terminus in the 1 ns time frame of the HDAC1−inhibitor complexes.

potential for differentiating between HDAC1, HDAC3, and HDAC8, while a differentiation of HDAC1 and HDAC2 will be more difficult. The finding that the selectivity of previously known isoform specific inhibitors can be reproduced and rationalized indicates that this computationally efficient method could be used to screen larger virtual libraries of HDAC for isoform selectivity. This is demonstrated by identification of NVP-LAQ824 as a potentially isoform selective inhibitor.

Analysis of the docked structures and the results from MD simulations using a nonbonded model for the metal

complexation are in agreement with these qualitative considerations. In addition, they provide insights into the balance between binding to the metal and interactions in the channel and on the surface. Optimization of the interactions in the channel and on the surface that take the flexibility of the protein into account could therefore counteract the weaker metal binding of a monodentate ligand, providing alternatives to the currently used hydroxamic acids binding units. The design, synthesis, and evaluation of novel HDAC inhibitors that make use of these principles is currently in progress and will be reported in due course.

**Acknowledgment.** We thank the Walther Cancer Institute for collaboration in this research. Support for computational resources from the National Science Foundation (DMR0079647) and the Office of Information Technology of the University of Notre Dame is also gratefully acknowledged.

**Supporting Information Available:** PROCHECK and WHATIF results for the four homology models, convergence, and stability plots for the MD simulations, dihedral angle plots for TSA, SK-683, and CG-1521, force field parameters and RESP charges of TSA, SK683, and CG-1521 as well as coordinates of the four homology models (pdb format) are available free of charge via the Internet at http://pubs.acs.org. The structures of the HDAC−inhibitor complexes are available from the authors upon request.

## References

(1) Pazin, M. J.; Kadonaga, J. T. What is up and down with histone deacetylation and transcription? *Cell* **1997**, *89*, 325−328. (b) Pennisi, E. Opening the way to gene activity. *Science* **1997**, *275*, 155−157.

(2) Yoshida, M.; Kijima, M.; Akita, M.; Beppu, T. Potent and specific inhibition of mammalian histone deacetylases both *in vivo* and *in vitro* by trichostatin A. *J. Biol. Chem.* **1990**, *265*, 17174−17179.

(3) Han, J. W.; Ahn, S. H.; Park, S. H.; Wang, S. Y.; Bae, G. U.; Seo, D. W.; Known, H. K.; Hong, S.; Lee, Y. W.; Lee, H. W. Apicidin, a histone deacetylase inhibitor, inhibits proliferation of tumor cells via induction of p21WAF1/Cip1 and gelsolin. *Cancer Res.* **2000**, *60*, 6068−6074.

(4) Kijima, M.; Yoshida, M.; Suguta, K.; Horinouchi, S.; Beppu, T. Trapoxin, an antitumor cyclic tetrapeptide, Is an irreversible inhibitor of mammalian histone deacetylases. *J. Biol. Chem.* **1993**, *268*, 22429−22435.

(5) Jung, M.; Brosh, G.; Kölle, D.; Schef, H.; Gerhöuser, C.; Loidl, P. Amide analogues of trichostatin A as inhibitors of histone deacetylase and inducers of terminal cell differentiation. *J. Med. Chem.* **1999**, *42*, 4669−4679. (b) Jung, M.; Hoffmann, K.; Brosch, G.; Loidl, P. Analogues of Trichostatin A and Trapoxin B as histone deacetylase inhibitors. *Bioorg. Med. Chem. Lett.* **1997**, *7*, 1655−1658. (c) Suzuki, T.; Ando, T.; Tsuchiya, K.; Fukazawa, N.; Saito, A.; Mariko, Y.; Yamashita, T.; Nakanishi, O. Synthesis and histone deacetylase inhibitory activity of new benzamide derivatives. *J. Med. Chem.* **1999**, *42*, 3001−3003. (d) Furumai, R.; Komatsu, Y.; Nishino, N.; Khochbin, S.; Yoshida, M.; Horinouchi, S. Potent histone deacetylase inhibitors built from trichostatin A and cyclic tetrapeptide antibiotics including trapoxin. *Proc. Natl. Acad. Sci. U.S.A.* **2001**, *98*, 87−92. (e) Massa, S.; Mai, A.; Sbardella, G.; Esposito, M.; Ragno, R.; Loidl, P.; Brosch, G. 3-(4-Aroyl-*1H*-prrol-2-yl)-*N*-hydroxy-2-propenamides, a new class of synthetic histone deacetylase inhibitors. *J. Med. Chem.* **2001**, *44*, 2069−2072. (f) Lavoie, R.; Bouchain, G.; Frechette, S.; Woo, S. H.; Khalil, E. A.; Leit, S.; Fournel, M.; Yan, P. T.; Trachy-Bourget, M.-C.; Beaulieu, C.; Li, Z.; Besterman, J.; Jelorme, D. Design and synthesis of a novel class of histone deacetylase inhibitors. *Bioorg. Med. Chem. Lett.* **2001**, *11*, 2847−2850.

(6) Richon, V. M.; Emiliani, S.; Verdin, E.; Webb, Y.; Breslow, R.; Rifkind, R. A.; Marks, P. A. A class of hybrid polar inducers of transformed cell differentiation inhibits histone deacetylases. *Proc. Natl. Acad. Sci. U.S.A.* **1998**, *95*, 3003−3007.

(7) Wang, D.-F.; Wiest, O. G.; Helquist, P. Lan-Hargest, H.-Y.; Wiech, N. L. *J. Med. Chem.* **2004**, *47*, 3409−3417. (b) Wang, D.-F.; Wiest, O. G.; Helquist, P. Lan-Hargest, H.-Y.; Wiech, N. L. *Bioorg. Med. Chem. Lett.* **2004**, *14*, 707−711. (c) Lan-Hargest, H.-Y.; Kaufman, R. J.; Wiech, N. L. US Patent Appl. US2002-0143196. (d) Roy S, Packman K, Jeffrey R, Tenniswood M. Histone deacetylase inhibitors differentially stabilize acetylated p53 and induce cell cycle arrest or apoptosis in prostate cancer cells. *Cell Death Differ*. **2005**, *12*, 482−491. (e) de Ruijter AJ, Kemp S, Kramer G, Meinsma RJ, Kaufmann JO, Caron HN, van Kuilenburg AB. The novel histone deacetylase inhibitor BL1521 inhibits proliferation and induces apoptosis in neuroblastoma cells. *Biochem Pharmacol*. **2004**, *68*, 1279−1288.

(8) Cohen, L. A.; Amin, S.; Marks, P. A.; Rifkind, R. A.; Desai, D.; Richon, V. M. Chemoprevention of carcinogen-induced mammary tumorigenesis by the Hybrid Polar Cytodifferentiation agent, suberanilohydroxamic acid (SAHA) *Anticancer Res.* **1999**, *19*, 4999−5005. (b) Desai, D.; El-Nayoumy, K.; Amin, S. Chemopreventive efficacy of suberanilohydroxamic acid (SAHA), a cytodifferentiating agent, against tobacco-specfic nitrosamine 4-(methylinitros-amino)-1-(3-pyridyl)-1-butanone (NNK)-induced lung tumorigenesis in female A/J mice. Proc. *AACR* **1999**, *40*, 2396, abstr. 362.

(9) Miller, T. A.; Witter, D. J.; Belvedere, S. Histone deacetylase inhibitors *J. Med. Chem.* **2003**, *46*, 5096−5115 and reference therein. (b) Yoshida, M.; Matsuyama, A.; Komatsu, Y.; Nishino, N. From discovery to the coming generation of histone deacetylase inhibitors. *Curr. Med. Chem.* **2003**, *10*, 2351−2358.

(10) De Ruijter, A. J. M.; Van Gennip, A. H.; Caron, H. N.; Kemp, S.; Van Kuilenburg, A. B. P. Histone deacetylases(HDACs): characterization of the classical HDAC family. *Biochem. J.* **2003**, *370*, 737−749.

(11) Verdin, E.; Dequiedt, F.; Kasler, H. G. Class II histone deacetylases: versatile regulations. *Trends Genet.* **2003**, *19*, 286−293.

(12) Gregoretti, I.; Lee, Y.-M.; Goodson, H. V. Molecular Evolution of the Histone Deacetylase Family: Functional Implications of Phylogenetic Analysis. *J. Mol. Biol.* **2004**, *338,* 17−31.

(13) It should be mentioned that while class III HDACs do contain a conserved zinc ion, it is believed to be structural and is not part of the catalytic mechanism. Blander, G.; Guarente, L. The Sir2 family of protein deacetylases. *Annu. Rev. Biochem.* **2004**, *73*, 417−435.

(14) (a) Brehm, A.; Miska, E. A.; McCance, D. J.; Reid, J. L.; Bannister, A. J. Kouzarides, T. Retinoblastoma protein recruits histone deacetylase to repress transcription. *Nature* **1998**, *391*, 597. (b) Magnaghi, J. L.; Groisman, R.; Naguibneva, I.; Robin, P.; Lorain, S.; Le, V. J.; Toalen, F.; Trouche, D. Harel, B. A. Retinoblastoma protein represses transcription by recruiting a histone deacetylase. *Nature* **1998**, *391*, 601.

(15) (a)Lemercier, C.; Verdel, A.; Galloo, B.; Curtet, S.; Brocard, M. P.; Khochbin, S. mHDA1/HDAC5 histone deacetylase interacts with and represses MEF2A transcriptional activity. *J. Biol. Chem.* **2000**, *275*, 15594. (b) Miska, E. A.; Karlsson, C.; Langley, E.; Nielsen, S. J.; Pines, J. Kouzarides, T. HDAC4 deacetylase associates with and represses the MEF2 transcription factor. *EMBO J.* **1999**, *18*, 5099.

(16) Kouzarides, T. Acetylation: a regulatory modification to rival phosphorylation ? *EMBO J.* **2000**, *19*, 1176−1179.

(17) Finnin, M. S.; Donigian, J. R.; Cohen, A.; Richon, V. M.; Rifkind, R. A.; Marks, P. A.; Breslow, R.; Pavletich, N. P. Structures of a Histone Deacetylase Homologue Bound to the TSA and SAHA Inhibitors. *Nature* **1999**, *401*, 188−193.

(18) Somoza, J. R.; Skene, R. J.; Katz, B. A.; Mol, C.; Ho, J. D.; Jennings, A. J.; Luong, C.; Arvai, A.; Buggy, J. J.; Chi, E.; Tang, J.; Sang, B.-C.; Verner, E.; Wynands, R.; Leahy, E. M.; Dougan, D. R.; Snell, G.; Navre, M.; Knuth, M. W.; Swanson, R. V.; Mcree, D. E.; Tari, L. W. Structural Snapshots of Human HDAC8 Provide Insights Into the Class I Histone Deacetylases. *Structure* **2004**, *12*, 1325−1334. (b) Vannini, A.; Volpari, C.; Filocamo, G.; Caroli Casavola, E.; Brunetti, M.; Renzoni, D.; Chakravarty, P.; Paolini, C.; De Francesco, R.; Gallinari, P.; Steinckuhler, C.; Di Marco, S. Crystal Structure of a Eukaryotic Zn-Dependent Histone Deacetylase,Human HDAC8, Complexed with a Hydroxamic Acid Inhibitor. *Proc. Nat. Acad. Sci. U.S.A.* **2004**, *101*, 15064−15069.

(19) Yoshida, M.; Furumai, R.; Nishyama, M.; Komatsu, Y. Nishino, N.; Horinouchi, S. Histone deacetylase as a new target for cancer chemotherapy. *Cancer Chemother. Pharmacol.* **2001**, *48* (Suppl 1), S20−S26.

(20) Hillisch, A.; Pineda, L. F.; and Hilgenfeld, R. Utility of homology models in the drug discovery process. *Drug Discovery Today* **2004**, *9*, 659−669 and the references therein.

(21) Thompson, J. D.; Higgins, D. G.; Gibson, T. J. ClustalW: improving the sensitivity of progressive multiple sequence alignment through sequence weighting, position-specific gap penalties and weight matrix choice. *Nucleic Acids Res.* **1994**, *22*, 4673−4680.

(22) Hall, T. A. BioEdit: a user-friendly biological sequence alignment editor and analysis program for Windows 95/98/NT. *Nucleic Acids Symp. Ser.* **1999**, *41*, 95−98.

(23) Sali, A.; Blundell, T. L. Comparative protein modeling by satisfaction of spatial restraints. *J. Mol. Biol.* **1993**, *234*, 779−815. (b) Laskowski, R. A.; MacArthur, M. W.; Moss, D. S.;

Thornton, J. M. PROCHECK: a program to check the stereochemical quality of protein structures. *J. Appl. Crystallogr*. **1993**, *26*, 283−291. (c) Morris, A. L.; MacArthur, M. W.; Hutchinson, E. G.; Thornton, J. M. Stereochemical quality of protein structure coordinates. *Proteins* **1992**, *12*, 345−364.

(24) Morris, G. M.; Goodsell, D. S.; Halliday, R. S.; Huey, R.; Hart, W. E.; Belew, R. K.; Olson, A. J. Automated Docking Using a Lamarckian Genetic Algorithm and Empirical Binding Free Energy Function. *J. Comput. Chem.* **1998**, *19*, 1639−1662.

(25) AutoDockTools can be downloaded free of charge from this website, http://www. scripps.edu/pub/olson-web/doc/autodock/tools.html.

(26) Case, D. A.; Darden, T. A.; Cheatham, T. E., III; Simmerling, C. L.; Wang, J.; Duke, R. E.; Luo, R. E.; Merz, K. M.; Wang, B.; Pearlman, D. A.; Crowley, M.; Brozell, S.; Tsui, V.; Gohlke, H.; Mongan, J.; Hornak, V.; Cui, G.; Beroza, P.; Schafmeister, C.; Caldwell, J. W.; Ross, W. S.; Kollman, P. A. AMBER 8, University of California, San Francisco, 2004.

(27) Gaussian 98, A.9, M. J. Frisch, G. W. Trucks, H. B. Schlegel, G. E. Scuseria, M. A. Robb, J. R. Cheeseman, V. G. Zakrzewski, J. A. Montgomery, R. E., Jr.; Stratmann, J. C. Burant, S. Dapprich, J. M. Millam, A. D. Daniels, K. N. Kudin, M. C. Strain, O. Farkas, J. Tomasi, V. Barone, M. Cossi, R. Cammi, B. Mennucci, C. Pomelli, C. Adamo, S. Clifford, J. Ochterski, G. A. Petersson, P. Y. Ayala, Q. Cui, K. Morokuma, D. K. Malick, A. D. Rabuck, K. Raghavachari, J. B. Foresman, J. Cioslowski, J. V. Ortiz, A. G. Baboul, B. B. Stefanov, G. Liu, A. Liashenko, P. Piskorz, I. Komaromi, R. Gomperts, R. L. Martin, D. J. Fox, T. Keith, M. A. Al-Laham, C. Y. Peng, A. Nanayakkara, M. Challacombe, P. M. W. Gill, B. Johnson, W. Chen, M. W. Wong, J. L. Andres, C. Gonzalez, M. Head-Gordon, E. S. Replogle, J. A. Pople, Gaussian, Inc., Pittsburgh, PA, 1998.

(28) Rao, M. S.; Olson, A. J. Modelling of factor Xa-inhibitor complexes: a computational flexible docking approach. *Proteins* **1999**, *34*, 173−83. (b)Tummino, P. J.; Ferguson, D.; Jacobs, C. M.; Tait, B.; Hupe, L.; Lunney, E.; Hupe, D. Competitive inhibition of HIV-1 protease by biphenyl carboxylic acids. *Arch. Biochem. Biophys.* **1995**, *316*, 523−528.

(29) Sotriffer, C. A.; Flader, W.; Winger, R. H.; Rode, B. M.; Liedl, K. R.; Varga, J. M. Automated docking of ligands to antibodies: methods and applications. *Methods* **2000**, *20*, 280−291. (b) Stoddard, B. L.; Koshland, Jr.; D. E. Prediction of a receptor protein complex using a binary docking method. *Nature* **1992**, *358*, 774−776.

(30) Minke, W. E.; Diller, D. J.; Hol, W. G.; Verlinde C. L. The role of waters in docking strategies with incremental flexibility for carbohydrate derivatives: heat-labile enterotoxin, a multivalent test case. *J. Med. Chem.* **1999**, *42*, 1778−1788. (b) Laederach, A.; Dowd, M. K.; Coutinho, P. M.; Reilly, P. J. Automated Docking of Maltose, 2-Deoxymaltose, and Maltotetraose into the Soybean beta-Amylase Active Site. *Protein* **1999**, *37*, 166−175. (c) Bitomsky, W.; Wade, R. C. Docking of Glycosaminoglycans to Heparin-Binding Proteins: Validation for aFGF, bFGF, and Antithrombin and Application to IL-8. *J. Am. Chem. Soc.* **1999**, *121*, 3004−3013.

(31) Chang, Y. T.; Veitch, N. C.; Loew G. H. A Theoretical Study of Benzhydroxamic Acid Binding Modes in Horseradish Peroxidase. *J. Am. Chem. Soc.* **1998**, *120*, 5168−5178. Compare also: (b) Perola, E.; Xu, K.; Kollmeyer, T. M.; Kaufmann, S. H.; Prendergast, F. G.; Pang, Y.-P. Successful Virtual Screening of a Chemical Database for Farnesyltransferase Inhibitor Leads. *J. Med. Chem.* **2000**, *43*, 401−408.

(32) Stote, R. H.; Karplus, M. Zinc-binding in proteins and solution-a simple but accurate nonbonded representation. *Proteins* **1995**, *23*, 12−31. For an alternative parametrization, see: (b) Hu, X.; Shelver, W. H. Docking studies of matrix metalloproteinase inhibitors: zinc parameter optimization to improve the binding free energy prediction. *J. Mol. Graph. Mod.* **2003**, *22*, 115−126.

(33) Donini, O. A. T.; Kollman, P. A. Calculation and prediction of binding free energies for the matrix metalloproteinases. *J. Med. Chem.* **2000**, *43*, 4180−4188. (b) Terp, G. E.; Christensen, I. T.; Jorgensen, F. S. Structural differences of matrix metalloproteinases. Homology modeling and energy minimization of enzyme−substrate complexes. *J. Biomol. Struct. Dyn.* **2000**, *17*, 933−946.

(34) Bayly, C. I.; Cieplak, P.; Cornell, W. D.; Kollman, P. A. A Well-Behaved Electrostatic Potential Based Method Using Charge Restraints for Deriving Atomic Charges − the Resp Model. *J. Phys. Chem.* **1993**, *97*, 10269−10280.

(35) Jorgensen, W. L. Chandrasekhar, J.; Madura, J. D.; Impey, R. W.; Klein, M. L. Comparison of simple potential functions for simulating liquid water. *J. Chem. Phys.* **1983**, *79*, 926−935.

(36) Pearson, W. A. Rapid and Sensitive Sequence Comparison with FASTP and FASTA. *Methods Enzymol.* **1990**, *183*, 63−98.

(37) Ayer, D. E. Histone deacetylases: transcriptional repression with SIN-ers and NuRDs. *Trends Cell Biol.* **1999**, *9*, 193−198.

(38) Vriend, G.; Sander, C. Quality control of protein models: Directional atomic contact analysis. *J. Appl.* Cryst. **1993**, *26*, 47−60. WHAT IF Web Interface. http://swift.cmbi.kun.nl/WIWWWI/.

(39) Frishman, D.; Argos, P. 75% accuracy in protein secondary structure prediction *Proteins* **1995**, *27*, 329−335.

(40) Wang, D.-F.; Wiest, O. Manuscript in preparation.

(41) Hu E.; Dul E.; Sung C. M.; Chen Z.; Kirkpatrick R.; Zhang G. F.; Johanson K.; Liu R.; Lago A.; Hofmann G.; Macarron R.; de los Frailes M.; Perez P.; Krawiec J.; Winkler J.; Jaye M. Identification of novel isoform-selective inhibitors within class I histone deacetylases. *J. Pharmacol. Exp. Ther.* **2003**, *307*, 720−728.

(42) Remiszewski, S. W.; Sambucetti, L. C.; Bair, K. W.; Bontempo, J.; Cesarz, D.; Chandramouli, N.; Chen, R.; Cheung, M.; Cornell-Kennon, S.; Dean, K.; Diamantidis, G.; France, D.; Green, M. A.; Howell, K. L.; Kashi, R.; Kwon, P.; Lassota, P.; Martin, M. S.; Mou, Y.; Perez, L. B.; Sharma, S.; Smith, T.; Sorensen, E.; Taplin, F.; Trogani, N.; Versace, R.; Walker, H.; Weltchek-Engler, S.; Wood, A.; Wu, A.; Atadja, P. N-hydroxy-3-phenyl-2-propenamides as novel inhibitors of human histone deacetylase with in vivo antitumor activity: discovery of (2*E*)-*N*-hydroxy-3-[4-[[(2-hydroxyethyl)[2-(1*H*-indol-3-yl)ethyl]amino]methyl]phenyl]-2-propenamide (NVP-LAQ824). *J. Med. Chem.* **2003**, *46*, 4609−4624.

(43) Lu, Q.; Wang, D.-S.; Chen, C.-S.; Hu, Y.-D.; Chen, C.-S. Structure-Based Optimization of Phenylbutyrate-Derived Histone Deacetylase Inhibitors *J. Med. Chem.* **2005**, *48*, 5530−5535

JM0505011